Performance of phase plates on the XMaS beamline at the ESRF

L. Bouchenoire,[a,b]* S. D. Brown,[b,c] P. Thompson,[b,c] J. A. Duffy,[a] J. W. Taylor[a] and M. J. Cooper[a,b]

[a]Department of Physics, University of Warwick, Coventry CV4 7AL, UK, [b]XMaS, European Synchrotron Radiation Facility, 6 Rue Jules Horowitz, BP 220, 38043 Grenoble, France, and [c]Department of Physics, University of Liverpool, Oliver Lodge Laboratory, Oxford Street, Liverpool L69 7ZE, UK. E-mail: boucheno@esrf.fr

Two phase plates, a 0.78 mm-thick natural diamond and a 0.3 mm-thick synthetic diamond, were used to convert linearly polarized X-rays into a circularly polarized beam, to cover an energy range of 3–9 keV. The performance of these plates followed theoretical predictions as indicated by polarization analyses and X-ray magnetic circular dichroism measurements. The use of the device is illustrated by resonant magnetic reflectivity measurements on UAs/Co multilayers.

Keywords: instrumentation; X-ray phase plates; polarization; ferromagnetism.

1. Introduction

In this paper, polarization analysis and circular dichroism measurements are presented. They have been performed to characterize two phase plates, a 0.78 mm-thick natural diamond and a 0.3 mm-thick synthetic diamond, installed on the XMaS beamline, which is situated on a bending magnet at the ESRF. The synthetic diamond has also been used to study the ferromagnetism in a UAs/Co multilayer by reflectivity measurements at the uranium M_4 edge. Diffraction and reflectivity studies of ferromagnets are an integral part of the research program on XMaS. A comprehensive description of the instrumentation has recently been given by Brown *et al.* (2001). The facility specifically includes a 1 T switchable magnet and the phase plate, in order to facilitate studies of magnetization in ferromagnets.

Circularly or elliptically polarized X-rays are useful for X-ray studies of magnetization in ferromagnets in order to couple the small term in the cross section, which involves the magnetization (spin and/or orbital), with the much larger charge-scattering term with which this small term is in quadrature (Lovesey & Collins, 1996). The signal of magnetic origin may be isolated by reversing either the handedness of the circular polarization or the direction of the sample's magnetization. In hard magnetic materials, reversing the direction of magnetization is difficult and changing the polarization is the desirable alternative. Phase plates are used over a wide energy range. Diamond crystals are more commonly used for energies lower than 10 keV (Giles *et al.*, 1993; Pizzini *et al.*, 1998). Although silicon crystals were used down to 2.8 keV by Goulon *et al.* (1996) and Varga *et al.* (1997), they are normally used for energies of 10–50 keV (Golovchenko *et al.*, 1986). For higher-energy X-rays (>50 keV), germanium, used as a monolithic two-crystal phase plate, performed successfully in Compton scattering studies (Yanhke *et al.*, 1994; Venkataram *et al.*, 1998). A few insertion devices exist that can provide left and right circularly polarized X-rays, but most studies have relied on field reversal rather than polarization reversal.

The incident polarized radiation from the synchrotron can be converted into circular/elliptical polarization in three different ways: (i) viewing the synchrotron radiation source above or below the electron orbit, a technique well established on XMaS and elsewhere; (ii) using special insertion devices such as helical undulators (*e.g.* Kawata *et al.*, 1989; Elleaume, 1994) to produce elliptical polarization in the orbital plane; and (iii) using a perfect crystal X-ray phase plate to convert linear to elliptical polarization. The latter method has been proved to be successful in X-ray magnetic circular dichroism (XMCD) experiments (Giles *et al.*, 1994; Pizzini *et al.*, 1998; Hirano & Maruyama, 1997). Quarter-wave plates rely on the birefringence of perfect crystals close to the Bragg condition. Dynamical theory shows that birefringent materials introduce a phase shift Φ between the two orthogonal components E_σ and E_π of the incident plane wave, and these components therefore propagate through the crystal with different phase velocities. E_π is the component of the incident electric field that lies in the diffraction plane of the phase plate, and E_σ is orthogonal to the plane. If the two plane-wave components emerge phase shifted by exactly $\pi/2$, and $|E_\sigma|$ equals $|E_\pi|$, the radiation is circularly polarized.

2. Laue transmission phase plate

The polarization state of an X-ray beam may be characterized by Stokes–Poincaré parameters (Blume & Gibbs, 1988; Azzam & Bashara, 1989; Born & Wolf, 1999). If the diffraction planes of the birefringent crystal are inclined by an angle ψ with respect to the electric field of the incident linearly polarized X-ray beam, the circular polarization rate $P'_{\rm C}$ of the transmitted wave depends on the phase shift Φ between the two components E_σ and E_π through the relation

$$P'_{\rm C} = -\sin 2\Psi \sin \Phi. \tag{1}$$

The transmitted beam becomes fully circularly polarized when $\psi = 45^\circ$ and $\Phi = 90^\circ$. Far from the region of quasi-total reflection, the phase shift Φ between E_σ and E_π components depends on the crystal thickness and on the angular offset $\Delta\theta$ of the incident X-rays from the Bragg condition such that

$$\Phi = -\left(r_{\rm e}^2 \,{\rm Re}[F_h F_{\bar{h}}]\right)(2\pi V^2)^{-1}\left[\lambda^3 t \sin(2\theta_{\rm B})\right](\Delta\theta)^{-1}, \tag{2}$$

where t is the effective thickness, *i.e.* the beam path length in the crystal, $r_{\rm e}$ is the classical electron radius, V is the volume of the unit cell, F_h is the structure factor of the hkl reflection and $\theta_{\rm B}$ is the Bragg angle. Quarter-wave plate conditions can therefore be obtained by turning the crystal away from the Bragg condition by an angle

$$\Delta\theta_{\pi/2} = -r_{\rm e}^2 \,{\rm Re}[F_h F_{\bar{h}}]\,\pi^{-2} V^{-2} \lambda^3 t \sin(2\theta_{\rm B}). \tag{3}$$

The angular dependence of the circular polarization rate of (1) can then be simply expressed as a function of $\Delta\theta_{\pi/2}$ and $\Delta\theta$ as

$$P'_{\rm C}(\Delta\theta) = -P_1 \sin\left[(\pi/2)(\Delta\theta_{\pi/2}/\Delta\theta)\right], \tag{4}$$

where P_1 is the linear polarization rate of the incident beam ($P_1 < 1$, in practice). For an X-ray beam with effective angular divergence α, the function $P'_{\rm C}(\Delta\theta)$ must be convoluted with a Gaussian of width α. The effective beam divergence results from the monochromator bandwidth and the slits that define the beam. In order to minimize the effect of the beam divergence α on $P'_{\rm C}$, $\Delta\theta_{\pi/2}$ should be maximized so that it falls in a region where the phase shift Φ changes slowly with $\Delta\theta$. This can be achieved by increasing the crystal thickness, at the expense of the transmitted flux. $P'_1(\Delta\theta)$ can be expressed in a similar way as a function of the angular offset

$$P'_1(\Delta\theta) = -P_1 \cos\left[(\pi/2)(\Delta\theta_{\pi/2}/\Delta\theta)\right]. \tag{5}$$

3. Phase-plate characterization

The energy was tuned to 7.833 keV so that it corresponded to a 45° Bragg angle from the (006) reflection of the graphite polarization analyzer crystal. This energy, which was conveniently close to the Gd L_3 edge studied by XMCD measurements (see §4), was selected by a constant-exit water-cooled Si(111) double-bounce monochromator. The incident linearly polarized radiation was converted into circular polarization by a 0.78 mm-thick diamond crystal in Laue geometry. The $(11\bar{1})$ diffracting planes made an angle of 19.47° with the [111] direction, which is normal to the phase-plate surface. A scintillation detector measured the X-ray photons scattered from a 12 µm-thick kapton foil, which was used as an incident-beam monitor upstream of the phase plate. All our measurements were carried out on orbit; the orbit position was determined by vertically scanning the primary slits, which were set at 0.1×0.1 mm, and by monitoring the photons scattered at 90° horizontally by a 12 µm-thick kapton foil. The experiments were carried out using the most stable machine mode and with the vertically opening slits set symmetrically about the orbital plane. Under these conditions the net degree of circular polarization in the incident beam should be negligible 'on orbit' (ideally it will be zero with no beam movement), and this fact is indeed confirmed by our subsequent measurements.

The Stokes parameters were first evaluated by two programs: one developed by D. Laundy (personal communication) and one developed by C. Vettier (personal communication). The former calculates P_1 and P_C of the white beam coming from the bending magnet as a function of (i) the offset from the orbital plane and (ii) the vertical aperture of the primary slits. On orbit, P_C and P_2 are zero and we can deduce the value of the unpolarized component from the vertical slit gap. P_1 and P_{un} were 99.83% and 5.74%, respectively. The values of the linear component were then used as inputs to Vettier's program, which simulates the Stokes parameters after the monochromator. The degree of polarization was found to be 99.84% and 5.67% for P_1 and P_{un}, respectively.

The Stokes parameters were then measured using the polarization analyzer (PA). The graphite crystal was rotated about the beam by an angle ξ of −45°, 0°, 45° and 90°. P_1' is determined by integrating the rocking curves from $\xi = 90°$ and $\xi = 0°$, so that $P_1 = (I_{90°} - I_{0°})/(I_{90°} + I_{0°})$. P_2 is defined in a similar way by integrating the rocking curves from $\xi = 45°$ and $\xi = -45°$. The incident beam was characterized by polarization analysis with the phase plate removed. The unpolarized component, P_{un}, can be defined as $(1 - P_1^2 - P_2^2)^{1/2}$, where P_1 and P_2 are the incident linear polarization in the horizontal plane and the degree of incident linear polarization at an angle of 45° to the horizontal, respectively. The incident beam was found to be 99.9 (0.1)% linearly polarized and 5.2% unpolarized at this energy. The experimental data are therefore in good agreement with the model.

The polarization parameters P_1' and P_2' were then measured in the same way with the diamond in the beam. As it is impossible to measure directly the value of the unpolarized component coming out of the diamond, P_{un}' was modeled. Effectively, equations (4) and (5) give the numbers of linearly and circularly polarized photons after the phase plate. As P_2' is negligible compared with P_1' and P_C', P_{un}' can be defined by $(1 - P_1'^2 - P_C'^2)^{1/2}$. P_{un}' reaches almost 100% (Fig. 1*a*) close to the region of quasi-total reflection. We can say that the diamond 'depolarizes' the X-rays in this region. The values of P_{un}' were then used to calculate P_C', which is defined by $\pm(1 - P_1'^2 - P_2'^2 - P_{un}'^2)^{1/2}$, where P_1' and P_2' are measured with the PA. The experimental value of P_C' (dashed lines in Fig. 1*b*) was then compared with the theoretical P_C' (full line in Fig. 1*b*). The model was obtained by convoluting $P_C'(\Delta\theta)$ of (4) with a Gaussian function of 11 arcsec FWHM, which represents the effective divergence of the beam. The experimental P_C' agrees very well with the model, and the ambiguity in its sign is resolved by the model. Thus it was shown that the phase plate converted the 99.9 (0.1)% linear polarized incident beam into a 99.1 (0.1)% circular polarized beam for an offset angle of ±64 arcsec. At this angular position, about 9% of the beam was unpolarized.

4. XMCD measurements at the Gd L_3 edge on $GdCo_{2.5}$

XMCD measurements were performed at the Gd L_3 edge on a 5 µm $GdCo_{2.5}$ foil at room temperature. The measurements were carried out on orbit with the primary slits set at 0.2×2 mm. The experimental set-up is given in Fig. 2. The diamond used in the previous section to characterize the polarization of the beam was employed in the same geometry to produce the circularly polarized X-rays. The first ionization chamber (IC1), which was filled with air, measured the flux transmitted through the diamond. The $GdCo_{2.5}$ foil was mounted on the diffractometer at an angle of 45° with respect to the incident X-rays. At this energy, the transmission of the diamond crystal was 24%. The flux transmitted through the foil was measured by the second ion chamber, IC2, which was argon-filled. Both detectors operated with a 2000 V potential across a 8 mm ionization gap. The Gd L_3 total absorption of the $GdCo_{2.5}$ foil is shown in Fig. 3(*a*).

The XMCD measurements were carried out by magnetizing the sample foil with a 1 T magnetic field applied alternatively parallel or antiparallel to the incident beam. The dichroic signal, which is defined as the half difference in absorption $(\mu^+ - \mu^-)$ for the two hands of

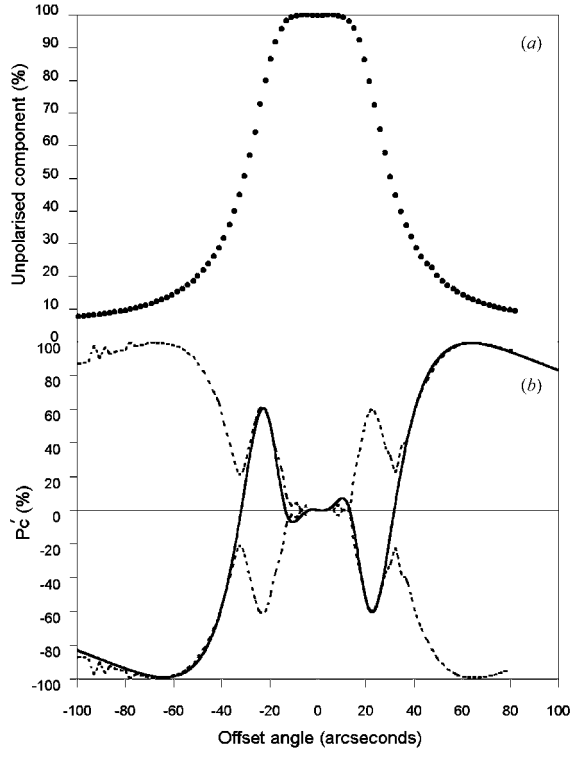

Figure 1
Unpolarized component deduced from theory (*a*) and circular polarization rate measured at 7.833 keV (*b*). The correct sign of the experimental $\pm P_C'$ (dashed line) is assigned from the modeled polarization of the phase plate (full line). The model is convoluted with a Gaussian function of width 11 arcsec (full line), which represents the effective divergence of the beam.

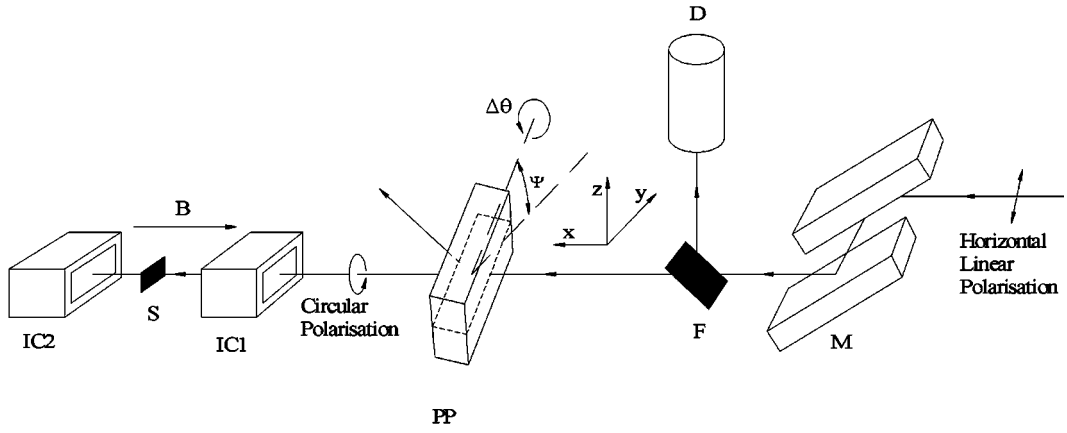

Figure 2
Schematic of the experimental set-up chosen for the XMCD measurements. M: Si(111) double-bounce monochromator. F: scattering foil. D: scintillation detector. PP: phase-plate. IC1 and IC2: ionization chambers. S: sample.

polarization, was obtained by (i) reversing the polarity of the magnetic field while keeping the helicity constant and subsequently by (ii) 'flipping' the helicity while keeping the magnetic field constant. The variation of the XMCD amplitude with $\Delta\theta$ is also a measure of the circular polarization rate. The measurements obtained in Fig. 4 were carried out at 7.246 keV, the energy for which the absorption is a maximum. The offset was varied between −100 and +100 arcsec and the magnetic field flipped at 10 s intervals. The angular offsets of ±79 and ±28 arcsec correspond to quarter-wave-plate and three-quarter-wave-plate conditions, respectively.

The maximum polarization rate obtained under quarter-wave-plate conditions is close to 99%, in agreement with the model that takes into account the effective divergence of the beam. Note that, compared with the previous section, the primary slit size was increased to maintain a high flux while enlarging the angular beam divergence.

The dichroic signal was then measured as a function of energy; the phase-plate offset was fixed at −79 arcsec, the angle for which P'_C is maximized at the Gd L_3 edge, and the field was flipped as the energy was tuned. The results are shown in Fig. 3(*b*). Note that for each energy the new Bragg angle was automatically recalculated but the offset angle did not need to be reset. For instance, for the highest energy (7.255 keV), the offset should have been 78.8 arcsec rather than 79 arcsec, but inspection of Fig. 4 shows that this change has a

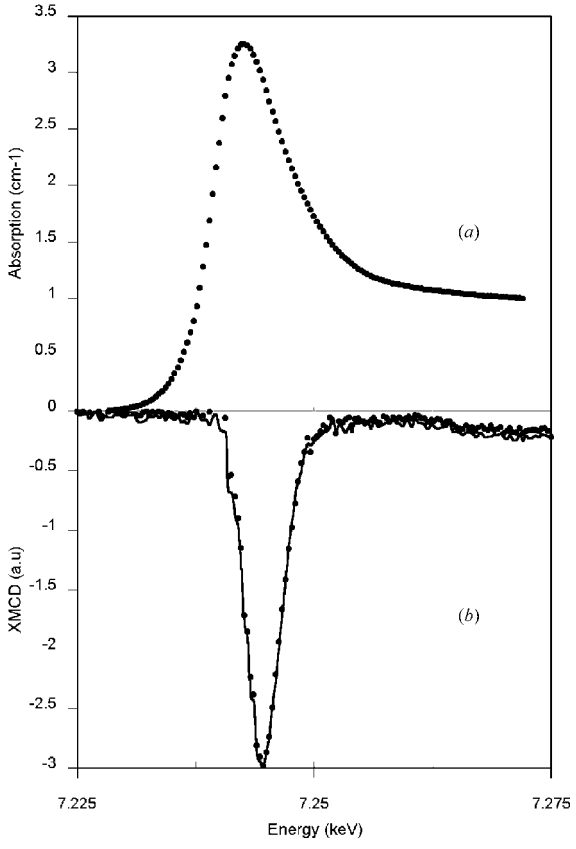

Figure 3
Gd L_3 absorption curve (*a*) and XMCD signal of $GdCo_{2.5}$ foil measured at room temperature (*b*) as a function of energy. The dichroic signal was measured when the magnetic field was 'flipped' and the helicity was kept constant (full line) and when the helicity was 'flipped' and the magnetic field was kept constant (dots).

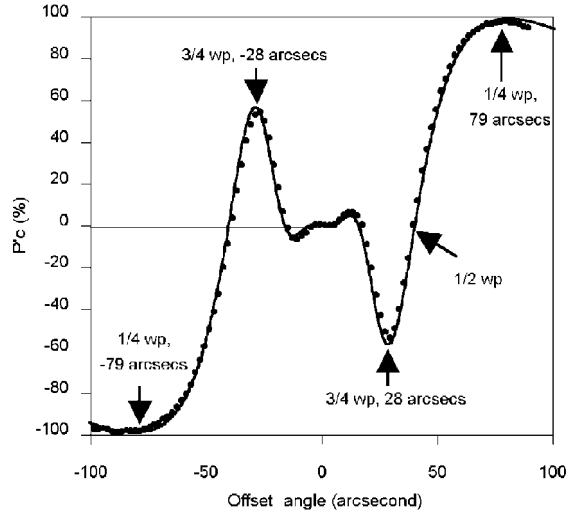

Figure 4
Angular dependence of the Gd L_3 edge XMCD amplitude (filled circles) obtained by field flipping The data are fitted to the modeled circular polarization, P'_C, which is given by (4) (full line) and is convoluted with a Gaussian function of 15 arcsec FWHM. Note that for this experiment the beam size was larger than in §3, and therefore the beam divergence is increased.

negligible effect on the degree of circular polarization. Fig. 3(*b*) proves that the XMCD signal is the same irrespective of whether the field (full line) or the helicity (dots) is reversed, which validates the operation of the phase plate. The results are also consistent with published data on $GdCo_5$ (Pizzini *et al.*, 1998).

5. Reflectivity measurements at the U M_4 edge on the UAs/Co multilayer

The phase plate was used for an investigation of the magnetic reflectivity of a $Co_{(200\ Å)}[U\text{-}As_{(80\ Å)}/Co_{(20\ Å)}]_{n=12}$ multilayer. This material is of particular interest because dichroism measurements (Sanchez *et al.*, 1998, 1999) revealed the existence of a magnetic moment on uranium at 35 K. For this experiment, a 300 µm-thick synthetic diamond was used to produce the circularly polarized X-rays necessary to undertake the reflectivity measurements. It was used in Laue geometry with the (111) diffracting planes making an angle of 35.26° with the [110] direction, which is perpendicular to the diamond surface. Without degrading the degree of circular polarization, primary slits as large as 0.5×10 mm were chosen to compensate for the loss in flux due to the low (∼1%) transmission of the diamond at the uranium M_4 edge (3.728 keV). The beam was measured to be 98.2 (0.1)% circularly polarized at an offset, $\Delta\theta$, of approximately 300 arcsec.

A standard two-stage closed-cycle He cryostat maintained the temperature of the thin film at 35 K. The sample was magnetized alternatively parallel or antiparallel to the incident beam with a 1 T magnetic field that was produced by a water-cooled electromagnet. The asymmetry ratio, R, represents the fractional change in intensity for each magnetic orientation and is defined as

$$R = (I^+ - I^-)/(I^+ + I^-). \quad (6)$$

This ratio was measured on reflection from the first superlattice peak of the multilayer by flipping the magnetic field at the maximum of left circular polarization that was produced by the diamond phase plate. This measurement was made for different energies near the uranium M_4 edge and the intensity of the reflected beam was recorded with an NaI scintillation counter. The results, which are depicted in Fig. 5(*b*), show that a magnetic signal of approximately −4.5% was measured in the $Co_{(200\ Å)}[U\text{-}As_{(80\ Å)}/Co_{(20\ Å)}]_{n=12}$ thin film with a counting time of ∼7 s at each setting. Interestingly, the maximum was found at 3.723 keV, *i.e.* 5 eV below the edge. This energy shift is not an energy calibration problem. The reflectivity was measured as a function of energy while the wavevector was kept constant (Fig. 5*a*). The dip at 3.727 keV, which originates from the strong uranium M_4 white-line absorption, confirms the validity of the energy calibration of the monochromator to within 1 eV. A magnetic 'dead layer' at the surface of the film (Bernhoeft *et al.*, 1998) may be responsible for this effect. If a non-magnetic layer exists on top of the ferromagnetic uranium, there will be no magnetic effect from this layer, but there will be a strong reduction in the penetration of the beam through the layer at the white-line energy and hence a much reduced dichroic signal, as observed.

The same measurements were repeated for the positive helicity with consistent results. The flipping ratio reached the same maximum value of +4.5% and at the same energy as for the negative helicity.

These measurements proved that it was possible to use the polarization produced by a diamond phase plate to measure a magnetic effect in reflection.

6. Conclusions

The results of polarization analyses and XMCD measurements show that the phase plates installed on XMaS perform as predicted. The reflectivity measurements demonstrate the application of this technique to a class of materials whose magnetic properties are of great interest, and for which there is a relative lack of other data. Similar work is being carried out on $[U_x/Fe_y]_n$ type multilayers for different temperatures.

The XMaS phase plate was built principally to undertake diffraction experiments on ferromagnets. Other phase-plate crystals will be acquired in order to cover an energy range of up to 15 keV, which is the upper limit afforded by the beamline toroidal mirror (Brown *et al.*, 2001), and to optimize the performance in the 3–4 keV region of the actinide M edges.

We thank S. Pizzini of the Louis Néel Laboratory (CNRS, Grenoble) for providing the $GdCo_{2.5}$ sample used to characterize our phase plate, and ESRF for the loan of the natural diamond crystal. We thank Professor W. G. Stirling, Dr C. A. Lucas (XMaS), C. Detlefs (ESRF) and other beamline staff for many useful discussions. We are grateful to the Engineering and Physical Sciences Research Council in the UK for funding the XMaS beamline facility through the universities of Liverpool and Warwick. We are extremely grateful to the referees for their detailed comments on the paper.

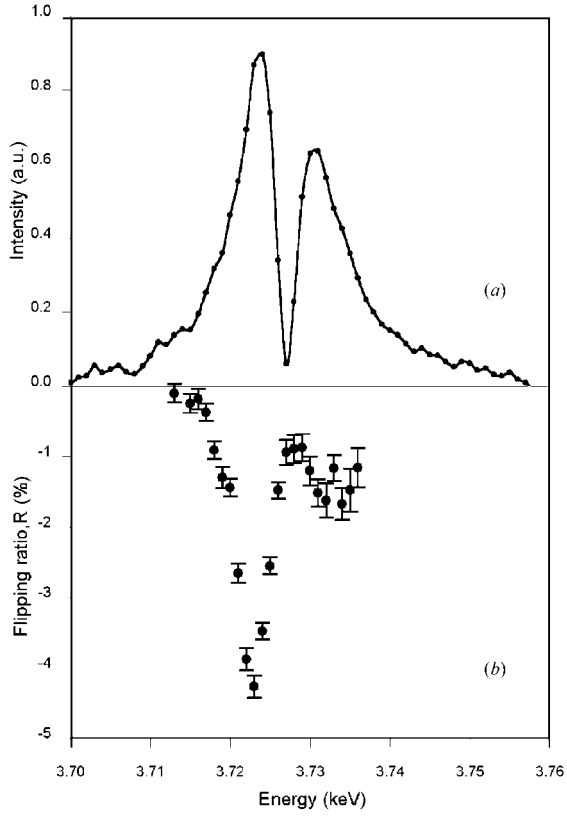

Figure 5
Reflectivity as a function of energy (*a*) and asymmetry ratio measured on $Co_{(200\ Å)}[U\text{-}As_{(80\ Å)}/Co_{(20\ Å)}]_{n=12}$ at the uranium M_4 edge with a negative helicity (*b*).

References

Azzam, R. M. A. & Bashara, N. M. (1989). *Ellipsometry and Polarized Light.* Amsterdam: North-Holland.

Bernhoeft, N., Hiess, A., Langridge, S., Stunault, A., Wermeille, D., Vettier, C., Lander, G. H., Huth, M., Jourdan, M. & Adrian, H. (1998). *Phys. Rev. Lett.* **81**, 3419–3422.

Blume, M. & Gibbs, D. (1988). *Phys. Rev. B*, **37**, 1779–1789.

Born, M. & Wolf, E. (1999). *Principles of Optics*, 7th ed. New York: Pergamon.

Brown, S. D., Bouchenoire, L., Bowyer, D., Kervin, J., Laundy, D., Longfield, M. J., Mannix, D., Paul, D. F., Stunault, A., Thompson, P., Cooper, M. J., Lucas, C. A. & Stirling, W. G. (2001). *J. Synchrotron Rad.* **8**, 1172–1181.

Elleaume, P. (1994). *J. Synchrotron Rad.* **1**, 19–26.

Giles, C. G., Malgrange, C., Goulon, J., de Bergevin, F., Vettier, C., Dartyge, E., Fontain, A., Giorgetti, C. & Pizzini, S. (1994). *J. Appl. Cryst.* **27**, 232–240.

Giles, C. G., Malgrange, C., Goulon, J., Vettier, C., de Bergevin, F., Freund, A. & Elleaume, P. (1993). *Proc. SPIE*, **2010**, 136–149.

Golovchenko, J. A., Kincaid, B. M., Levesque, R. A., Meixner, A. E. & Kaplan, D. R. (1986). *Phys. Rev. Lett.* **57**, 202–205.

Goulon, J., Malgrange, C., Giles, C., Neumann, C., Rogalev, A., Moguiline, E., de Bergevin, F. & Vettier, C. (1996). *J. Synchrotron Rad.* **3**, 272–281.

Hirano, K. & Maruyama, H. (1997). *Jpn. Appl. Phys.* **36**, L1272–L1274.

Kawata, H., Miyahara, T., Yamamoto, S., Shioys T., Kitamura H., Sato, S., Kananaya, N., Lida, A., Mikiuni, A., Sat, M., Iwazumi, T., Kitajima, Y. & Ando, M. (1989). *Rev. Sci. Instrum.* **60**, 1885–1888.

Lovesey, S. W. & Collins, S. P. (1996). *X-ray Scattering and Absorption by Magnetic Materials.* Oxford: Clarendon.

Pizzini, S., Bonfin, M., Baudelet, F., Tolentino, H., San Miguel, A., Mackay, K., Malgrange, C., Hagelstein, M. & Fontaine, A. (1998). *J. Synchrotron Rad.* **5**, 1298–1303.

Sanchez, J. P., Dalmas de Roetier, P., Kernavois, N., Mannix, D., Stirling, W. G. & Yaouane, A. (1998). ESRF, Experimental Report Number HE226. ESRF, Grenoble, France.

Sanchez, J. P., Dalmas de Roetier, P., Kernavois, N., Mannix, D., Stirling, W. G. & Yaouane, A. (1999). ESRF, Experimental Report Number HE420. ESRF, Grenoble, France.

Varga, L., Giles, C., Neumann, C., Rogalev, A., Malgrange, C., Goulon, J. & de Bergevin, F. (1997). *J. Phys. IV*, **7**, C2-309–313.

Venkataram, C. T., Lang, J. C., Nelson, C. S., Srajer, G., Haeffner, D. R. & Shastri, S. D. (1998). *Rev. Sci. Instrum.* **69**, 1970–1973.

Yanhke, C. J., Srajer, G., Haeffner, D. R., Mills, D. M. & Assoufid, L. (1994). *Nucl. Instrum. Methods A*, **347**, 128–133.